Direct kinetic simulation of ion acoustic turbulence in cathode plume

IEPC-2017-496

Presented at the 35th International Electric Propulsion Conference
Georgia Institute of Technology • Atlanta, Georgia • USA
October 8 – 12, 2017

Kentaro Hara[1]
Texas A&M University, College Station, Texas, 77843, USA

and

Kenichi Kubota[2]
Japan Aerospace Exploration Agency, Chofu, Tokyo, 182-8522, Japan

Abstract: One dimensional kinetic simulations of current carrying plasma in the vicinity of a Hollow cathode plume are performed. Ion acoustic instabilities are investigated using collisionless Vlasov simulations with periodic boundary conditions for different ratios of electron bulk velocity to the thermal velocity (called the electron Mach number in this paper). It is observed from the simulations that the ion trapping only occurs at positive phase velocity when the electron Mach number is below 1.25, which is consistent with the linear perturbation theory. When the electron Mach number increases, the magnitude of the plasma wave increases and ion trapping is observed at both positive and negative velocities of the ion acoustic speed. This suggests that a large-amplitude plasma wave is excited due to the large electron bulk velocity. Preliminary calculations show that the collisional DK simulation produces the transition from collisional to collisionless regimes in hollow cathode plasma.

I.Introduction

Hollow cathode plays an important role in electric propulsion operations, particularly for Hall effect thrusters. Understanding the hollow cathode physics is essential in advancing the EP devices because (i) cathode coupling voltage is important in determining the thruster efficiency, (ii) the cathode oscillation modes affect the thruster body operation, (iii) cathode erosion is one of the main lifetime limiting factors for EP missions as the magnetically shielded Hall thrusters significantly improves the lifetime of the thruster body, and (iv) extending and improving the hollow cathodes will be more critical with higher power thrusters.

The main simulation codes available for cathode study in the EP community have been fully fluid[1] or hybrid fluid-PIC[2] simulation methods. Both of these methods employ fluid electron model, in which anomalous mobility term is added to the elastic and inelastic collisions. The simulation results taking the anomalous mobility into account are very promising and show good agreement with experimental data[3]. However, there is no study to date of a fully kinetic simulation that directly shows the linear growth and saturation of the instability as well as the velocity distribution functions of the ions and electrons during this process. In this paper, a one-dimensional direct kinetic (DK) simulation is used to model the current carrying plasma. Kinetic equations, such as the Vlasov and Boltzmann-type equations, are solved directly in discretized phase space. This method has been used for plasma sheaths[4], Hall thruster discharge plasma[5], and various plasma wave simulations[6,7]. It has been shown that the DK method can be advantageous over particle-based kinetic method, i.e. particle-in-cell (PIC) method, since the statistical noise inherent due to the use of

---

[1] Assistant Professor, Department of Aerospace Engineering, khara@tamu.edu.
[2] Researcher, Aeronautical Technology Directorate, kkubota@chofu.jaxa.jp.

macroparticles is essentially eliminated in the DK method. Here, the DK method is used for both the ions and electrons, and is coupled with the Poisson solver assuming that there is no magnetic field applied to or induced in the system.

While a dense collisional plasma is created and the neutral atom density is large inside the hollow cathode, the plasma density in the downstream outside of the orifice exit of the keeper can be three orders of magnitude smaller[8]. Therefore, the momentum-transfer collision frequencies due to intermolecular collisions, such as the electron-neutral, electron-ion Coulomb, and ion-ion Coulomb collisions, drastically drop from the inside to the outside of the cathode. The discharge plasma in hollow cathodes is typically assumed to be nonmagnetized unless the magnetic fields from the thruster body interacts with the cathode. Assuming the Ohm's law, $\vec{E} = \eta\vec{j}$, if the electron current density is constant, the electric field is proportional to the resistivity, hence to the momentum-transfer collision frequency ($\eta = m_e\nu/e^2n$). For a small momentum-transfer collision frequency, the Joule heating ($\vec{j}\cdot\vec{E}$) decreases. Computer simulations of hollow cathode discharge plasmas show that an anomalous electron resistivity is required to obtain the plume structure observed from experiments[1]. Recent experimental studies confirmed the existence of ion acoustic turbulence[9], which is considered to be the source of the anomalous electron transport. It is also reported that high energy ions are generated up to 100 eV downstream of the hollow cathode plume, while a typical discharge voltage is 20 V[10,11].

Despite the success of electron fluid models for the hollow cathode plasmas, a fully kinetic model can be of use to investigate the linear growth and nonlinear saturation of the ion acoustic instability due to the electron current carrying configuration. In particular, the ion kinetics cannot be taken into account using a fluid model. In this paper, we show that high energy ions can be generated due to the ion acoustic instability, which may play an important effect in erosion of the hollow cathode.

II.Current-carrying instability

Current-carrying instability is a fundamental plasma physics problem that can be derived from linear dispersion relation. Assuming the velocity distribution function (VDF) $f = f_0 + f_1$, where f_0 is the equilibrium VDF and f_1 is the perturbed component ($f_1/f_0 \ll 1$). For analyzing small amplitude waves, the perturbation components are assumed to follow $f_1 \propto \exp\left[i\left(\vec{k}\cdot\vec{x} - \omega t\right)\right]$, where $\vec{k}$ is the wave vector, $\vec{x}$ is the position, ω is the frequency, and t is the time. In this definition, $\omega = \omega_r + i\gamma$, where ω_r and γ are the real part of the frequency and growth rate, respectively. To model current-carrying instability, electrons and singly-charged ions are taken into account. The equilibrium electron and ion VDFs are assumed to be Maxwellian:

$$f_{0,e}(v_e) = n\sqrt{\frac{1}{\pi v_{th,e}}}\exp\left[-\frac{(v_e - U_e)^2}{v_{th,e}^2}\right],$$

and

$$f_{0,i}(v_i) = n\sqrt{\frac{1}{\pi v_{th,i}}}\exp\left(-\frac{v_i^2}{v_{th,e}^2}\right),$$

where n is the number density, v_{th}, v, and U are thermal velocity, particle velocity, and bulk (drift) velocity, and subscript i and e denote ions and electrons, respectively. Here, $v_{th} = \sqrt{k_BT/m}$, where k_B is the Boltzmann constant, T is the temperature, and m is the mass. The dispersion relation of this system is given by

$$1 = \frac{Z'(\xi_e)}{2(k\lambda_{De})^2} + \frac{Z'(\xi_i)}{2(k\lambda_{De})^2}, \tag{1}$$

where Z is the plasma dispersion function, $\lambda_{De} = v_{th,e}/\omega_{pe}$ is the Debye length, and $\xi_e = \frac{\omega}{kv_{th,e}} - \frac{U_e}{v_{th,e}}$ and $\xi_i = \frac{\omega}{kv_{th,i}}$. Stringer shows the same dispersion relation, and uses look up tables of the plasma dispersion relation to evaluate the real frequency and growth rate[12]. A common procedure that is used[13] is to assume that the phase velocity of the wave is much less than the electron thermal speed ($\omega \ll kv_{th,e}$) and much greater than the ion thermal speed ($\omega \gg kv_{th,i}$). If $|\xi_e| < 1$ and $|\xi_i| > 1$, the dispersion relation yields

$$\frac{\gamma}{\omega_r} \approx -\sqrt{\frac{\pi}{8}}\left[\sqrt{\frac{m_e}{m_i}}\left(1-\frac{U_e}{c_s}\right)+\left(\frac{T_e}{T_i}\right)^{3/2}\exp\left(-\frac{T_e}{2T_i}\right)\right],$$
$$\frac{\omega_r}{k} \approx +c_s, \tag{2}$$

where $c_s = \sqrt{\frac{k_B T_e}{m_i}}$ is the ion acoustic speed. For $U_e \gg c_s$,

$$\frac{\gamma}{\omega_r} \approx \sqrt{\frac{\pi}{8}}\left[M-\left(\frac{T_e}{T_i}\right)^{\frac{3}{2}}\exp\left(-\frac{T_e}{2T_i}\right)\right], \tag{3}$$

where M is defined in this paper as

$$M = \frac{U_e}{v_{th,e}}. \tag{4}$$

Eq. (3) means that $\gamma \approx \omega_r$. Note that $|\xi_e| < 1$ is equivalent to $U_e - v_{th,e} < \frac{\omega}{k} < U_e + v_{th,e}$. If $\omega_r = kc_s$, this approximation is valid for $U_e < c_s + v_{th,e}$. Therefore, it is expected that this dispersion relation is only valid for $U_e \leq v_{th,e}$, i.e., $M \leq 1$.

In the absence of electron drift ($U_e = 0$), the dispersion relation becomes

$$1+\frac{1}{(k\lambda_{De})^2}-\frac{\omega_{pi}^2}{\omega^2} = 0,$$

assuming $v_{th,i} \ll \frac{\omega}{k} \ll v_{th,e}$. In the limit of $k\lambda_D \ll 1$, this results in $\omega^2 = k^2 c_s^2$, namely,

$$\frac{\omega}{k} = \pm c_s. \tag{5}$$

It can be seen that the ion acoustic wave propagates in both directions, i.e., isotropically, when there is no electron drift.

Another extreme is when the electron-to-ion drift is larger than the ion and electron thermal velocities, namely, $U_e \gg v_{th,e}$ and $U_e \gg v_{th,i}$. Two streaming ion and electron beams experiencing ion acoustic type wave, which is called the Buneman instability[14,15]. The dispersion relation is given by

$$1-\frac{\omega_{pe}^2}{(\omega-kU_e)^2}-\frac{\omega_{pi}^2}{\omega^2} = 0.$$

The real frequency and growth rate at the resonance, $kU_e = \omega_{pe}$, are

$$\frac{\omega_r}{k} \approx \frac{1}{2}\left(\frac{m_e}{2m_i}\right)^{\frac{1}{3}}\left[1+\frac{1}{2}\left(\frac{m_e}{2m_i}\right)^{\frac{1}{3}}\right]U_e \approx \frac{1}{2}\left(\frac{m_e}{2m_i}\right)^{\frac{1}{3}}U_e, \tag{6}$$

$$\gamma \approx \frac{\sqrt{3}}{2}\left(\frac{m_e}{2m_i}\right)^{\frac{1}{3}}\left[1-\frac{1}{2}\left(\frac{m_e}{2m_i}\right)^{\frac{1}{3}}\right]\omega_{pe} \ll \omega_{pe}. \tag{7}$$

The growth and nonlinear saturation of this instability was extensively studied in Ref. 15. It was shown that the nonlinear saturation occurs due to the ion trapping by the ion acoustic wave.

Finally, taking the ion and electron temperature contributions into account, the dispersion relation is given by

$$1-\frac{\omega_{pe}^2}{\left(\omega-kU_e-ikv_{th,e}\right)^2}-\frac{\omega_{pi}^2}{\left(\omega-ikv_{th,i}\right)^2} = 0.$$

Assuming $\frac{\omega}{k} \ll U_e$, the solution to this dispersion relation can be obtained as

$$\frac{\omega_r}{k} \approx c_s, \tag{8}$$

$$\gamma \approx k\left(\frac{m_e}{m_i}\right)^{\frac{1}{2}}\left[U_e-\left(\frac{T_i}{T_e}\right)^{\frac{1}{2}}v_{th,e}\right]. \tag{9}$$

At resonance (see Ref. 12), $kU_e \approx \omega_{pe}$, the fastest growing growth rate is

$$\gamma \approx \omega_{pi}\left[1-\left(\frac{T_i}{T_e}\right)^{\frac{1}{2}}\frac{1}{M}\right],$$

which is dependent on the electron Mach number.

Note that all the growth rate and real frequency obtained under different situations are based on linear perturbation theory, which means that the perturbation of the VDF is small compared to the equilibrium VDF. Therefore, from the Poisson's equation, the electric field induced by the plasma wave is also assumed to be small, namely, small-amplitude approximation. Large-amplitude waves, i.e., when significant particle trapping occurs during the plasma wave generation needs to be investigated using nonlinear Vlasov-Poisson systems.

III.Direct-kinetic (DK) simulation

Linear growth and nonlinear saturation of current-carrying instability are investigated using a collisionless direct-kinetic (DK) simulation, in which the Vlasov-Poisson equations are solved. The one-dimensional (1D) Vlasov equation is given by

$$\frac{\partial f}{\partial t}+v\frac{\partial f}{\partial x}+\frac{qE(x)}{m}\frac{\partial f}{\partial v}=S,$$

where E is the electric field and S is the collision term. The 1D Poisson's equation is

$$\frac{\partial \phi^2}{\partial x^2}=-\frac{e}{\epsilon_0}(n_i-n_e),$$

where $n_i=\int f_i dv$ is the ion number density, $n_e=\int f_e dv$ is the electron number density, and ϕ is the potential. The Vlasov equation is solved in discrete phase space (physical and velocity space) using a finite volume method with monotonic upwind scheme for scalar conservation (MUSCL) framework with Strang's time splitting for the physical and velocity advection[16]. The boundary conditions developed in the DK method include Dirichlet, Neumann, and periodic boundary conditions. Also, several injection methods based on half-Maxwellian and shifted-Maxwellian are also developed. For a periodic boundary condition, a fast Fourier transform (FFT) solver is used for the Poisson solve. For the other boundary conditions, a tridiagonal matrix solver is used to handle Dirichlet and Neumann conditions.

The first set of simulations include investigation of collisionless current carrying instability in a 1D periodic box. The initial condition is as follows. (1) The ions are stationary, follow a Maxwellian distribution, and the ion temperature is 0.2 eV. (2) The electrons are shifted Maxwellian where the bulk velocity can be chosen (current carrying), and the electron temperature is 2 eV. Therefore, T_i/T_e = 0.1. (3) The number densities of ions and electrons are equal, i.e. quasineutral plasma. The electron current density is fixed and the plasma density can be varied, so that the bulk velocity changes. As the electron temperature is fixed, this results in changing the ratio of electron bulk velocity to the thermal electron velocity, which we call the electron Mach number throughout this paper. The grid size is chosen to be approximately 10-15 grids per Debye length and the time step is 0.1 ps to resolve the fastest motion, i.e., due to electrons. The simulation domain covers 130 Debye lengths so that multiple wave modes can be excited and it runs up to 2.5 – 5 µs. The velocity space for ions and electrons is $\pm 36\ v_{th,i}$ and $\pm 16\ v_{th,e}$, and singly-charged argon ions are assumed. The number of grid points in the velocity space is 1800 and 1200 for ions and electrons, respectively. The second set of simulations are more realistic simulations of hollow cathode plume, in which electron-electron, electron-ion, ion-ion Coulomb collisions and ionization source are added. The collisions are simplified using a Bhatnagar–Gross–Krook (BGK) collision model[17]. The purpose of the 2nd set of simulations is to investigate the transition between collisional and collisionless regions in the cathode plasma. The simulation runs on a Texas A&M University ada cluster for 6-8 hours using 36 processors. Message-Passing Interface (MPI) is used for parallel computing.

IV.Collisionless current-carrying instability

Using periodic boundary conditions, we investigated the collisionless current-carrying instabilities for different electron Mach numbers. The electron Mach numbers ($M=U_e/v_{th,e}$) are varied from 1 to 2.5.

A. Comparison with theory

Figure 1 shows the overall summary of the comparisons between several Mach numbers. The instability goes through three phases. First, there is a period where the electric field is low before the linear instability is excited. The numerical simulations show that it takes longer time for the lower Mach number cases to initiate the ion acoustic instabilities, while the instability occurs within the first 100 ns for $M \geq 1.5$. For this reason, no ion acoustic instability was observed for $M \leq 1.1$ within our 5 μs simulations. To observe an ion acoustic instability for $M \leq 1.1$, a higher noise level (add some perturbation) for the initial condition or a finer grid (the numerical errors may be dampening the instability growth) may be needed. The velocity bin for electrons is Δv = 7500 m/s might be causing a numerical error that keeps instability to grow. The time required for the ion acoustic instability to initiate might, however, be physical because the low velocity particles are more likely to experience Coulomb collisions and thermalize. One possibility is that the frequency of electron thermalization around the phase velocity needs to be compared with the instability growth rate. Second, the linear growth occurs when the wave energy grows exponentially, as can be clearly seen from the insert in Fig. 1. The linear growth rate can be obtained numerically from taking the slope. Finally, nonlinear saturation of the plasma wave is followed by the linear growth, in which the magnitude of the wave stays relatively constant. It can be seen that the higher electron Mach number cases result in larger saturation electric field (electrostatic energy).

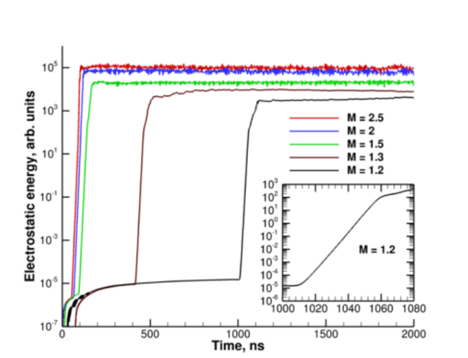

Figure 1. The electrostatic energy for different electron Mach number cases. Insert shows a zoomed-up view of the linear growth for M=1.2.

The growth rate of the ion acoustic instabilities can be calculated from Fig. 1 following $\frac{d\epsilon}{dt} = 2\gamma\epsilon$, where ϵ is the electrostatic energy density. From our calculations, the growth rate of $M = 1.2$ is 1.67×10^8 s^{-1} and that of $M = 2.5$ is 1.81×10^8 s^{-1}. From Eq. (3), the growth rate can be obtained analytically. The initial ion number density is 9.32×10^{18} m^{-3} for the $M = 1.2$ case and 4.5×10^{18} m^{-3} for $M = 2.5$ case. The growth rates obtained from the analytical solution are shown in Table 1. The numerical results agree well with the analytical solutions in terms of the order of magnitude. The qualitative trend is also same in that the growth rate increases as the electron Mach number increases. The difference between the numerical and analytical growth rates for the $M = 1.2$ is 15 %. However, the discrepancy become larger at $M = 2.5$, the plasma wave is no longer small-amplitude waves. It is likely that nonlinear effects play a role for higher electron Mach numbers.

Table 1. Growth rate comparison. Note that plasma density is assumed to be O(10^{18}-10^{19} m^{-3}).

	Numerical	Analytical
M = 1.2	1.67×10^8 s^{-1}	1.97×10^8 s^{-1}
M = 2.5	1.81×10^8 s^{-1}	3.17×10^8 s^{-1}

B. Small Mach number cases

Figure 2 shows the initial (0 s) and steady-state (3 μs) ion VDFs for $M = 1.2$. The initial VDF is a Maxwellian and after the ion acoustic wave initiates the ion trapping occurs near the phase velocity. The ion acoustic speed for the present simulation ($T_e = 2$ eV) is 2100 m/s. However, it can be seen that the ion trapping occurs around a higher velocity, e.g., 4000 m/s. As shown in Figs.1(a) and 1(b) in Ref. 12, the phase velocity of the ion acoustic wave for which the growth rate is largest has can be larger than the ion acoustic speed itself. The phase velocity lies between c_s and 5 c_s, for hydrogen plasma depending on T_i/T_e and $M = U_e/v_{th,e}$. Also note that the dispersion relation described in Section II is only under small-amplitude limit and for $U_e \leq v_{th,e}$. Thus, the discrepancy between the phase velocity obtained in the numerical simulation and the simplified theory (Eq. (2)) is expected and a more complete theory is required.

Commented [Office1]:

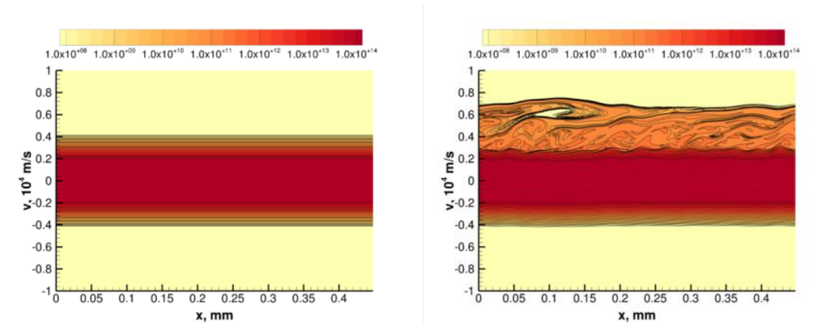

(a) 0 ns (Initial) (b) 3 μs

Figure 2. The ion VDFs for M =1.2 Note that the color map is in log scale.

The trapped ion population is 5-6 orders of magnitude smaller than the maximum peak of the VDFs. Therefore, it is difficult to capture the ion trapping due to ion acoustic wave with a particle-based simulation because the number of macroparticles per cell needs to be 10^5 or more to resolve such a small VDF. Although not shown in this paper, this is confirmed using a collisionless particle-in-cell (PIC) simulation. One advantage of a grid-based kinetic method, such as the DK method, is to resolve such small signals in the phase space. Complex structure of the ion phase space can be seen, i.e., the waves excited near the phase velocity (4,000 m/s) and low wave number (large wave length) modes exist. Merging of the plasma waves, i.e., decay of the plasma waves, is a signature of ion acoustic waves[18]. Since the wave number at which the growth rate is maximum is a broadband spectrum, the plasma wave can be excited at different wave numbers.

Figure 3 shows the temporal evolution of the electric field and electron bulk velocity for the $M = 1.2$ case. The electric field at 3000 ns corresponds to the ion VDF shown in Fig. 2(b). The electric field grows quickly from 1000 ns to 1100 ns, as shown in Fig. 1. From Stringer, the wave number at which the growth rate is at maximum is approximately

$$\frac{kU_e}{\omega_{pe}} \approx 1.$$

Thus, the wave length is

$$L = \frac{2\pi}{k} = \frac{2\pi U_e}{\omega_{pe}} = 2\pi \frac{U_e}{v_{th,e}} \lambda_{De} = 2\pi M \lambda_{De}. \tag{10}$$

It can be seen that there are approximately 11 modes (numerical) at t=1500 ns in Fig. 3(a), and Eq. (10) predicts $n = L_{domain}/L$ =12 (analytical), which are in good agreement. The number of modes reduces to 10 at t = 3000 ns, which is likely to be a consequence of phase mixing of trapped ions.

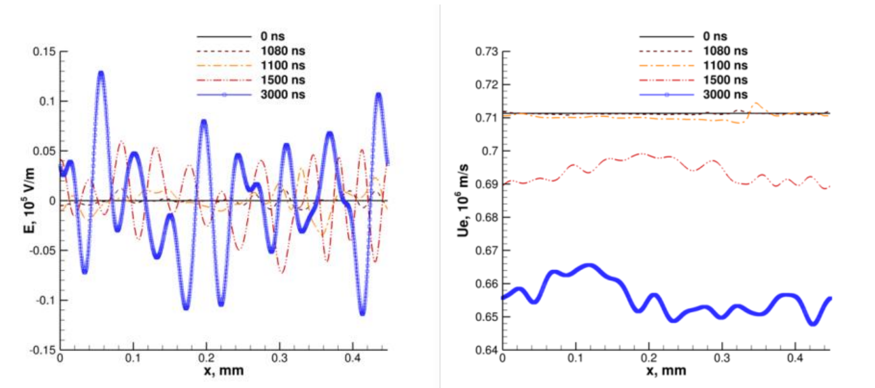

(a) Electric field (b) Electron bulk velocity

Figure 3. Plasma properties during linear instability and nonlinear saturation for M=1.2

As shown in Fig. 3(b), the electron bulk velocity decreases during the ion acoustic instability. The difference in the electron bulk velocities from the initial condition to the steady-state (3 μs) is 9.5%. This is because the electrons also are trapped around the phase velocity of the plasma wave, which is at $\omega/k \approx 4000$ m/s. Once electron trapping occurs, the slower and faster electrons around the phase velocity will be exchanged via the plasma wave and plateau in the VDF appears (e.g., Landau damping). Although it is difficult to see from the static figures in the paper, the electric field indeed propagates in the +x direction, which is consistent with the phase velocity of plasma wave only having the positive value.

Figure 4 shows the electron VDFs of $M = 1.2$. It can be seen that the trapping width of the electrons is much smaller than the thermal velocity of the electron Maxwellian in $M = 1.2$, indicating that magnitude of the plasma wave is smaller than $T_e = 2$ eV. It can be therefore seen that at $M = 1.2$ the linear perturbation theory still holds because the electric field is small enough and the plasma wave is not too large to perturb the bulk distribution of the plasma constituents. It is important to note that the positive phase velocity (no trapping observed around the negative phase velocity) is consistent with the linear perturbation theory described in Section II.

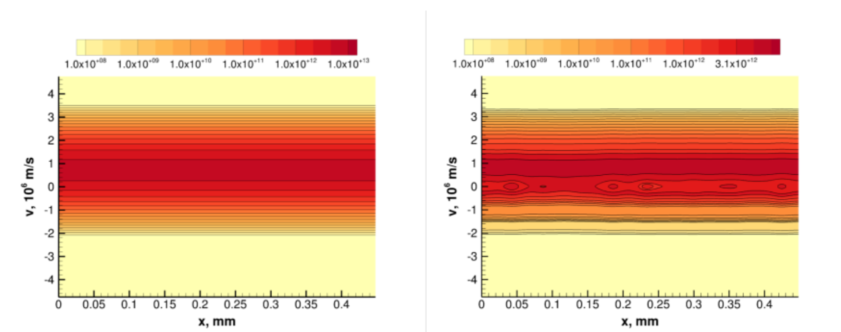

(a) 0 s for M=1.2 (b) 3 μs for M=1.2*

Figure 4. Electron trapping around the phase velocity, i.e., ion acoustic velocity, resulting in collisionless electron drag for M = 1.2. The color map is in log scale. (*) Note that two contour lines are added around the trapped particle region in Fig. 4(b) to illustrate the particle trapping.

The electron trapping occurs around $v = 4000$ m/s (very small value in the electron VDF scale 10^6 m/s), which causes the bulk velocity to decrease. Thus, collisionless drag occurs via the generation of ion acoustic waves. Also note that the electron VDF is broadened, i.e., the electrons are thermalized, due to the electron trapping. This results in the effective electron Mach number (bulk velocity / thermal velocity) to reduce even more.

C. Large Mach number cases

Figure 5 shows the time evolution of the ion VDFs for $M = 2$. As the electron bulk velocity (U_e) becomes larger than the electron thermal velocity ($v_{th,e}$), it can be expected that the free energy that the electron current possesses is larger so that the ion acoustic instability becomes more nonlinear. The broadband feature of the ion acoustic wave can be seen from the waves with small and large wave numbers (not a coherent single mode) being excited. One thing that is remarkable is the appearance of ion trapping in the negative velocity. Because of the positive and negative velocity components, the plasma wave as a whole acts more like a standing wave rather than a traveling wave. At later time (see Fig. 5(c)), due to phase mixing (numerical and physical), the fine structures of the trapped particles are dissipated, which makes the spatially-averaged ion VDFs flatter. The bulk VDFs also experience a large perturbation from the plasma wave.

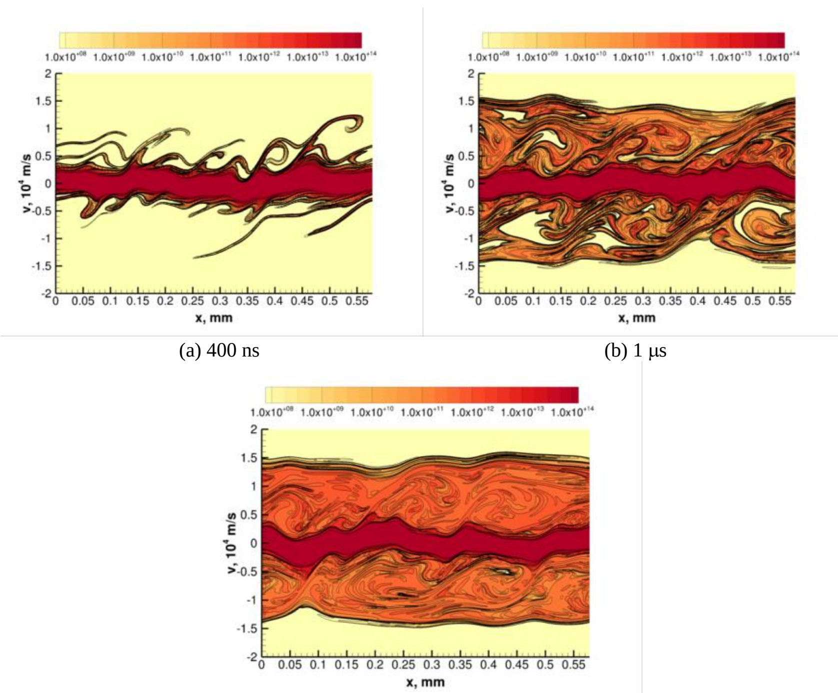

(a) 400 ns (b) 1 μs

(c) 2 μs

Figure 5. Ion VDFs for M = 2. Note that the color map is in log scale.

The reason why this is important for hollow cathode is that high energy ions can be transporting back to the cathode, and hence contribute to erosion of the cathode orifice and other components. For $M = 2$, i.e., $U_e = 2v_{th,e}$, therefore the kinetic energy of electrons is $\frac{1}{2}m_e U_e^2 = 4$ eV in addition to the electron temperature 2 eV. The maximum ion velocity generated via ion acoustic instability at $M = 2$ is $v_i = 1.5 \times 10^4$ m/s, which corresponds to an ion energy of 47 eV. It is equally important to note that the trapped ion population is a few orders of magnitude smaller than the bulk of the ion VDF. For the overall erosion rate, higher energy ions have much larger impact than lower energy ions, because there is typically a threshold energy below which sputtering of the material does not occur. Therefore, it would be important to account for the high-energy ions generated via ion acoustic waves for cathode erosion study. Note that the change in ion bulk velocity before and after the ion acoustic instability is negligible because the bulk of the ion VDF is not affected. Only the kinetic effects around the phase velocity play an important role.

As shown in Fig. 1, the growth rate of the ion acoustic instability obtained from the present simulations is on the order of 100 MHz (here the plasma density is 5×10^{18} m^{-3} and argon is assumed), so the electrons have enough bounce cycles for the trapping to complete. Note that the growth rate of the ion acoustic wave depends on the electron temperature and the wave number at which the growth rate is at maximum. The electron bounce frequency for a sinusoidal plasma wave[19] is given by $\omega_{B,e} = \sqrt{ekE_0/m_e}$, where k is the wave number and E_0 is the electric field amplitude. The bounce frequency is approximately 30 GHz assuming $E_0 = 10^5$ V/m and $k = \frac{\omega_{pe}}{U_e} = 4.55\times10^4$ m^{-1}. Therefore, the electrons have 10^3-10^4 times of bounce cycles when the ion acoustic instability is in the linear growth mode. On the other hand, the ion bounce frequency is given by $\omega_{B,i} = \sqrt{m_e/m_i}\omega_{B,e}$, which is approximately 140 MHz. As shown in Fig. 5(a), ions are not fully trapped (the bounce motion is not completed), and it takes another 4-5 bounce cycles to be fully trapped (see Fig. 5(b) at 1 μs). Additionally, it is known that 2D plasma wave propagation is much more complex and the wave front can bow in or out depending on the conditions[20]. A 2D fully kinetic simulation is reserved for future work.

Commented [Office2]:

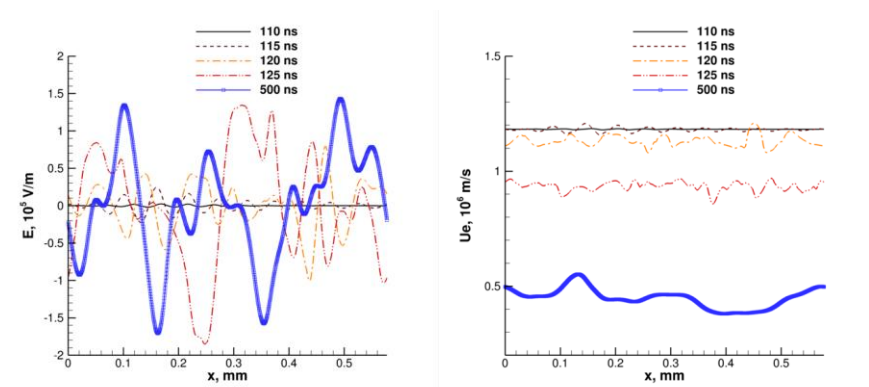

(a) Electric field (b) Electron bulk velocity

Figure 6. Plasma properties during linear instability and nonlinear saturation for M = 2.

Figure 6 shows the time evolution of the plasma properties, namely, the electric field and the electron bulk velocity, for the $M = 2$ case. The instability occurs within a few 10s of nanoseconds, from 110 ns to 130 ns. In comparison to the lower Mach number case in Fig. 3, the plasma wave is not a single mode and has multiple wave lengths. Also, the plasma waves act more like a standing wave rather than a traveling wave because of the two counterstreaming waves due to ion acoustic waves. The electron bulk velocity at 500 ns is approximately 38 % of the initial bulk velocity since the electron trapping due to ion acoustic wave results in significant collisionless electron drag. The kinetic energy of electrons transfer into (i) electron heating due to non-Maxwellian effects, (ii) generation of high energy ions (thermalization of ions), and (iii) generation of electrostatic energy of the plasma wave. The total energy, i.e., the sum of the energy of ions and electrons as well as the electrostatic energy, is conserved.

D. Discussion

The reason why the ion trapping region is large is because of the electric field amplitude (plasma wave) and the phase velocity of the ion acoustic wave. Stringer's theory predicts that the phase velocity is on the order of the ion acoustic speed ($c_s = \sqrt{k_B T_e / m_i}$), however, it also shows that the coefficient can vary ($\omega/k = \alpha c_s$), where $\alpha = O(10^{-1}) - O(10)$. In our simulations, the ion acoustic speed is fixed at 2190 m/s because $T_e = 2$ eV and m_i =40 amu. This means that ion trapping would occur around $v = c_s = 2190$ m/s if $\alpha = 1$.

Let us examine Fig. 2, i.e., $M = 1.2$. The ion trapping occurs roughly around the phase velocity $\omega/k = 4000$ m/s, which is about twice larger than the ion acoustic speed. Note that the ion VDF at 4000 m/s is initially $\exp(-v_i^2/2k_B T_i) \sim 10^{-8}$ times smaller than that of the peak VDF, therefore, there are essentially no particle in that velocity range. Since this phase velocity $v_i = 4000$ m/s corresponds to an ion energy of $0.5 m_i v_i^2$ = 3.3 eV, the magnitude of the plasma wave must be 3.3 V if the plasma wave only has a single wave number. Here, it can be seen from Fig. 3(a) that the magnitude of the plasma wave is less than 1 V on average, which suggests that the ions are accelerated to a velocity higher than the phase velocity (4000 m/s) by a plasma wave with multiple wave numbers, i.e., ion acoustic turbulence, hence creating locally a high potential drop that achieves sufficient ion trapping. For a large M, the electron kinetic energy due to the drift is immediately converted into thermal energy due to electron trapping. As the electron temperature becomes significant with respect to the drift energy, it is likely that the dispersion relation reduces to the conventional ion acoustic wave (see Eq.(5)) and the phase velocities appear in both directions, for which the dispersion relation needs to be modified.

Commented [Office3]:

In comparing Fig. 3 ($M = 1.2$) and Fig. 6 ($M = 2$), the electron bulk velocity for the lower Mach number ($M = 1.2$) is initially smaller but becomes larger after saturation of the ion acoustic instability than the initially high Mach number ($M = 2$). Hence, the process in which the hollow cathode plasma achieves steady state will be particularly important if the ion acoustic instability is in the nonlinear saturation regime.

V.Collisional-to-collisionless transition in hollow cathode plume

Two simulations were conducted to model the transition from collisional and collisionless regimes in the hollow cathode discharge plasma. Several trials were made but we present two cases that showcase the development of 1D hollow cathode model.

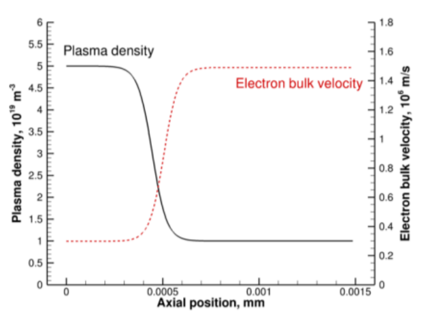

Figure 7. Initial condition for the collisional DK simulation.

Here, a quasi-1D flow, in which the boundary conditions are electron injecting (cathode side) and electron absorbing surfaces (anode side), is considered. A small voltage drop of 3 V is applied between the two boundaries. The electron current is fixed at 30 A, assuming 2 mm radius plasma channel. The constant electron current density is injected from the cathode surface, which results in electron flux (Γ_e) of 1.5×10^{25} m^{-2} s^{-1}. The injection from the anode surface follows a Neumann condition for both ions and electrons. The plasma density is assumed to be 5×10^{19} m^{-3} and 1×10^{19} m^{-3} at the cathode and anode sides, respectively, and the resulting electron bulk velocity ($U_e = \Gamma_e / n_e$) as shown in Fig. 7. The electron temperature is assumed to be 2 eV, so that the electron Mach number ($M = U_e / v_{th,e}$) varies from 0.5 to 2.5. Therefore, it is expected that the ion acoustic instability occurs at the higher M region. Neutral atom density is assumed to follow the same shape as the initial plasma density as shown in Fig. 7 but with a magnitude of 10^{21} m^{-3} in the cathode side and 2×10^{20} m^{-3} in the anode side. To model ion-ion, electron-ion, electron-electron Coulomb collisions, simplified collision operator such as a BGK model is added. The rate coefficients for Coulomb collision are calculated based on the plasma formulary. Here, T_i = 0.2 eV and T_e = 2 eV were assumed. We plan to add more realistic collision operators in future work. Ionization and radial diffusion loss are also taken into account.

Figure 8 shows a case when ion-ion Coulomb collision is an order of magnitude higher than the actual collision frequency. To maintain the ion density profile similar to the initial condition, ions are produced and/or lost accordingly. The ion VDFs are near-Maxwellian, so no ion trapping was observed. Since the electrons that are injected from the anode side follows Neumann condition, particle trapping needs to occur at a positive phase velocity, say 1x10^6 m/s in this result, to maintain the electron current conservation. Because the electron phase velocity is positive, the electric field is finite in the collisionless region. Additionally, due to current conservation, the electron bulk velocity is low where the plasma density is large. Ion acoustic instability occurs in the downstream region where the plasma density drops. This can be seen from the electron trapping from the electron phase space. Note that an electron sheath is formed near x = 0, also because the potential drop between two boundaries is assumed to be 3 V. While the potential drop occurs in the collisionless region (x>0.6 mm) and the density gradient region (0.4 < x < 0.6 mm), the cathode potential is larger than the bulk plasma potential around x = 0.2 mm.

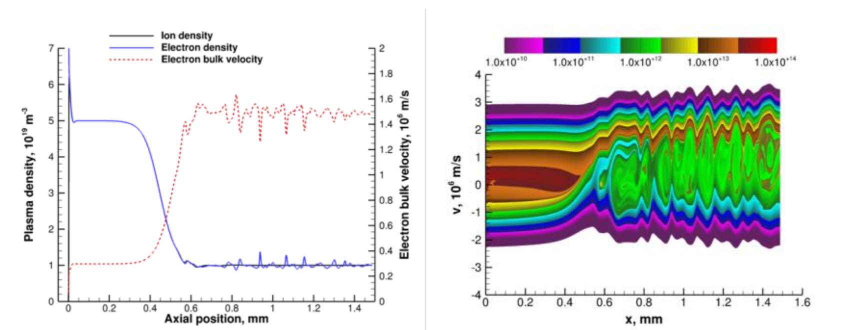

(a) Plasma profile (b) Electron phase space

Figure 8. Results at t=100ns for collisional ion case.

The following is reserved for future work: (i) larger domain, say 2 cm, in 1D, (ii) neutral atom density profile from other fluid simulations, and (iii) collision models with reconstruction of the post-collision VDFs based on macroscopic fluid quantities. Modeling of the ion density is particularly important because the electrons like to maintain quasineutrality and the electron density varies the electron bulk velocity, assuming the current density stays constant. However, the ion dynamics is determined by ionization and radial diffusion loss that are both slow time scale phenomena. To obtain a true steady-state simulation, computational time must be further extended from 1 μs.

VI.Conclusions

Collisionless and collisional direct kinetic (DK) simulations are conducted for ion acoustic instabilities due to electron current, which may occur in a hollow cathode plume. Using the collisionless DK simulations, current-carrying ion acoustic instabilities are investigated. The ratio between the electron bulk velocity and electron thermal velocity (here, for convenience this quantity is defined as electron Mach number ($M = U_e/v_{th,e}$) is varied to study the kinetic effects on ions and electrons.

The electron Mach number below 1.25 shows that the ion trapping only occurs around the positive ion acoustic velocity, which agrees with the linear perturbation theory. This is consistent with the fact that the magnitude of the plasma wave, i.e., the potential fluctuation, is considerably smaller than the electron temperature. In our simulations, it was shown that the linear growth of the instability does not initiate right after the start of the simulation and the time required for the initiation of the ion acoustic instability has some correlation with the electron Mach number. This will be further investigated. On the other hand, when the electron Mach number is larger than 1.25, the perturbation become large enough and the ion acoustic instability excites a large-amplitude plasma wave. The magnitude of the plasma wave is large so that the electron trapping significantly perturbs the bulk distribution. The most remarkable result is that the ion trapping occurs in both positive and negative phase velocities, which is a signature of the "ion acoustic wave" in the absence of electron drift. The maximum ion energy due to ion acoustic instability increases exponentially with the magnitude of the plasma wave, which is dependent on the initial electron Mach number. Even if the population of these high-energy ions is considerably smaller than the bulk ion VDF, these particles can contribute to sputtering of the material because the energy is higher than the threshold energies of sputtering.

Preliminary calculations of the more realistic hollow cathode plasma are performed including collisions. From the calculations, the collisional-to-collisionless transition was observed, in which the electron trapping and plasma wave occurs at the lower plasma density, i.e., larger electron bulk velocity region, downstream of the hollow cathode plume. More simulations will be carried out including collision operators, larger domain, and more physical boundary conditions. A fully kinetic simulation can be useful for investigating the high-energy ion generation via ion acoustic instabilities.

Acknowledgments

The authors thank Shinatora Cho for useful discussions on the plasma modeling, Marcel Georgin for gratefully sharing literature on hollow cathode plasmas, Texas A&M University's Supercomputing facilities (ada cluster) for the run times, and Brian Puckett, a NSF Research Experience for Undergraduate (REU) student, for running and developing post-processing tools for the collisionless simulations.

References

[1] I. G. Mikellides, I. Katz, D. M. Goebel, and K. K. Jameson, Journal of Applied Physics **101**, 063301 (2007).
[2] K. Kubota, Y. Oshio, H. Watanabe, S. Cho, Y. Ohkawa, and I. Funaki, "Numerical and Experimental Study on Discharge Characteristics of High-Current Hollow Cathode", AIAA-2016-4628, 52nd AIAA/SAE/ASEE Joint Propulsion Conference, Salt Lake City, UT, 2016.
[3] I. G. Mikellides, I. Katz, D. M. Goebel, and K. K. Jameson, "Evidence of Non-classical Plasma Transport in Hollow Cathodes for Electric Propulsion", Journal of Applied Physics **101**, 063301 (2007).
[4] K. Hanquist, K. Hara, and I. D. Boyd, "Detailed Modeling of Electron Emission for Transpiration Cooling of Hypersonic Vehicles," Journal of Applied Physics **121**, 053302 (2017).
[5] K. Hara, M. J. Sekerak, I. D. Boyd, and A. D. Gallimore, Journal of Applied Physics **115**, No. 20 (2014).
[6] K. Hara, T. Chapman, J. W. Banks, S. Brunner, I. Joseph, R. L. Berger, and I. D. Boyd, "Quantitative study of trapped particle bunching instability in Langmuir waves", Physics of Plasmas 22, 022104 (2015).
[7] K. Hara, I. Barth, E. Kaminski, I. Y. Dodin, and N. J. Fisch, "Kinetic simulations of ladder climbing' by electron plasma waves", Physical Review E, 95, 053212 (2017).
[8] K. Kubota, Y. Oshio, H. Watanabe, S. Cho, Y. Ohkawa, and I. Funaki, "Hybrid-PIC Simulation on Plasma Flow of Hollow Cathode", Trans. JSASS Aerospace Tech. Japan **14**, Pb_189-Pb_195 (2016).
[9] B. A. Jorns, I. G. Mikellides, and D. M. Goebel, Physical Review E **90**, 063106 (2014).
[10] D. M. Goebel, K. K. Jameson, I. Katz, and I. G. Mikellides, "Potential fluctuations and energetic ion production in hollow cathode discharges," Physics of Plasmas **14**, 103508 (2007).
[11] R. E. Thomas, H. Kamhawi, and G. J. Williams, Jr, "High Current Hollow Cathode Plasma Plume Measurements", IEPC-2013-076, 2013.
[12] T. E. Stringer, "Electrostatic instabilities in current-carrying and counterstreaming plasmas", J. Nucl. Energy, Part C Plasma Phys. **6** 267 (1964).
[13] R. Fitzpatrick, "Plasma Physics: An Introduction", CRC Press, Taylor & Francis Group, 2014.
[14] O. Ishihara, A. Hirose, and A. B. Langdon, "Nonlinear evolution of Buneman instability", Physics of Fluids **24**, 452 (1981).

[15] K. Hara, I. D. Kaganovich, and E. A. Startsev, "Generation of forerunner electron beam during interaction of ion beam pulse with plasma", (in review).
[16] K. Hara, Ph.D. Dissertation, University of Michigan (2015).
[17] P. L. Bhatnagar, E. P. Gross, and M. Krook, Physical Review 94, 511 (1954).
[18] T. Chapman, S. Brunner, J. W. Banks, R. L. Berger, B. I. Cohen, and E. A. Williams, "New insights into the decay of ion waves to turbulence, ion heating, and soliton generation," Physics of Plasmas 21, 042107 (2014).
[19] R. L. Berger, S. Brunner, T. Chapman, L. Divol, C. H. Still, and E. J. Valeo, "Electron and ion kinetic effects on non-linearly driven electron plasma and ion acoustic waves", Physics of Plasmas **20**, 032107 (2013).
[20] J. W. Banks, R. L. Berger, S. Brunner, B. I. Cohen, and J. A. F. Hittinger, "Two-dimensional Vlasov simulation of electron plasma wave trapping, wave front bowing, self-focusing, and sideloss", Physics of Plasmas **18**, 052102 (2011).